Nuclear Instruments and Methods in Physics Research B 409 (2017) 116–120

Contents lists available at ScienceDirect

Nuclear Instruments and Methods in Physics Research B

journal homepage: www.elsevier.com/locate/nimb

Positioning of cobalt atoms in amorphous carbon films by pre-selecting the hydrogen concentration

P. Gupta [a,b], G.V.M. Williams [b,c], S. Vajandar [d], T. Osipowicz [d], H.-W. Becker [e], K.-H. Heining [f], R. Hübner [f], J. Leveneur [a,b], J. Kennedy [a,b], A. Markwitz [a,b,*]

[a] National Isotope Centre, GNS Science, Lower Hutt, New Zealand
[b] The MacDiarmid Institute for Advanced Materials and Nanotechnology, Victoria University, Wellington, New Zealand
[c] School of Chemical and Physical Sciences, Victoria University, Wellington, New Zealand
[d] The Centre for Ion Beam Applications, Department of Physics, National University of Singapore, Singapore
[e] RUBION, Ruhr University, Bochum, Germany
[f] Institute of Ion Beam Physics and Materials Research, Helmholtz-Zentrum, Dresden-Rossendorf, Germany

ARTICLE INFO

Article history:
Received 13 December 2016
Received in revised form 27 March 2017
Accepted 1 April 2017
Available online 14 June 2017

Keywords:
Cobalt implantation
Diamond-like carbon
Hydrogen
Bimodal distribution
Atomic positioning

ABSTRACT

Amorphous carbon and hydrogenated amorphous carbon layers were implanted at room temperature with Co ions to investigate the role of hydrogen on the Co distribution. Amorphous carbon (a:C) and hydrogenated amorphous carbon (a:C–H) films were prepared by mass selective ion beam deposition with a 5 kV acceleration voltage using C^+ and $C_3H_6^+$ ions, respectively. The typically 100 nm thin films were implanted with Co using a 30 kV acceleration voltage to a fluence of 4×10^{16} cm^{-2}. Raman measurements showed that Co implantation in hydrogenated amorphous carbon causes increased sp^2 clustering while in amorphous carbon there is significant rehybridisation of carbon from sp^3 to sp^2 bonding. High resolution Rutherford backscattering measurements indicated that in the absence of hydrogen in the base matrix, the implantation profile assumes a unimodal distribution as predicted by simulations. However, in the presence of hydrogen the effects of collision cascade enhanced diffusion are significant in altering the implantation profile resulting in a bimodal distribution. The difference in the Co depth distribution between a:C and a:C–H films is explained by the change in thermal conductivity of the carbon matrix in the presence of hydrogen. The ability to position Co (magnetic atoms) in the surface region of diamond-like carbon films offers great advantages for applications in novel magnetic devices.

1. Introduction

Ion-solid interaction is a matter of significant interest to the materials industry. The distribution of mono-energetic ions in a material is generally described by a unimodal profile. However, significant deviations in the implantation profiles are observed when factors other than ballistics play a key role. For example, collision cascade enhanced diffusion and nanoparticle formation has reported to cause a bimodal distribution in thermal insulators such as silica and silicon dioxide [1–3]. In our recent work we reported a bimodal distribution of Co implanted into hydrogenated amorphous carbon at an implantation energy and current density as low as 30 keV and 5 μA cm^{-2} [4,5]. This was in contrast with earlier reports which either used a high implantation energy or high current density [1–3]. The same thermal insulators silica/silicon dioxide do not show a bimodal distribution at the implantation conditions reported in our work [6]. This difference was explained by the very low thermal conductivity of hydrogenated diamond-like carbon (DLC) (0.3 W/mK) compared to SiO_2 (3 W/mK) [4,5,7]. In this work we compare the distribution profile of cobalt in amorphous carbon which is reported to have a thermal conductivity of 1.5–3.5 W/mK with hydrogenated amorphous carbon [7]. This comparison will help in directly verifying the role of thermal conductivity and hydrogen in the distribution of implanted atoms in insulating matrices.

2. Methods

Both a:C and a:C–H films were fabricated by mass-selective ion beam deposition at GNS Science [8–10]. The system uses a Penning

* Corresponding author at: National Isotope Centre, GNS Science, Lower Hutt, New Zealand.
E-mail address: a.markwitz@gns.cri.nz (A. Markwitz).

http://dx.doi.org/10.1016/j.nimb.2017.04.005
0168-583X/

ion source coupled to an electromagnet for mass separation. Several focussing lenses are used throughout the transport column to focus the ion beam through the magnet and ultimately to the target stage in the sample chamber. Mass-selective ion beam deposition allows accurate control over the deposition energy and ion species which determine the mechanical properties, electrical properties, hydrogen content and sp^2/sp^3 ratio of the films [11]. The Penning ion source was operated with an anode voltage of 2 kV and a total terminal voltage of 5 kV to extract ion beams from the carbon rich plasma. An alternative means of producing thin films with the Penning ion source is by direct deposition which offers the opportunity to deposit large number of films on various substrates simultaneously [12]. Carbon monoxide and butane were used as precursor gases to generate C^+ and $C_3H_6^+$ ions for a:C and a:C–H film deposition, respectively. The ions were selected by passing the extracted ion beams to a 40 cm radius electromagnet which separates the ions based on mass, charge and energy. The mass resolution was further improved by the use of slits in the beam line. Together with a low base pressure of $\leq 5 \times 10^{-7}$ hPa in the sample chamber, high purity of the films is guaranteed. The deposition energy was set to 5 keV for a:C films. For a:C–H films, the 5 keV molecular ion $C_3H_6^+$ dissociates into individual atoms upon impact. The energy gets distributed among the dissociated species based on their mass [9]. The deposition energy is ~1400 eV and 120 eV for carbon and hydrogen ions, respectively. These films have a C:H ratio of 3:1 [10]. DLC films grow by the subplantation method resulting in the intermixing of deposited ions with substrate atoms in the first few layers [11]. The extent of this mixing depends on the ion energy. As the ion energy increases the extent of the intermixing layer, which in this case is between carbon and silicon, increases [8,10,12,13]. The thin films have to be sufficiently thick to minimise the contribution of silicon at the surface of the film [8,10,12,13]. Accordingly, the films are deposited to a thickness of 100 nm for a:C–H film and 200 nm for a:C films.

Cobalt ion implantation was carried out on the as-deposited films using the ion implanters at GNS Science in a similar setup [14]. Neon was used as the precursor gas in the Penning ion source to generate the plasma and to sputter Co ions from solid conductive Co sputter targets. The terminal voltage of the system was set to 30 kV to allow sub-surface penetration in the range of 25–35 nm within the films. The range was chosen so as to prevent accumulation of a significant fraction of Co at the surface avoiding opportunities for oxidation. Deeper penetration range was avoided to prevent Co atoms from reaching the interface to the silicon substrate. The implantation was carried out with a beam current of $\leq 5\ \mu A\ cm^{-2}$ to prevent any bulk heating effects on the sample. Both during deposition and implantation, the ion beam was raster scanned across a 11 mm × 11 mm aperture in both horizontal and vertical direction to ensure uniform coverage. Cobalt was implanted to a fluence of $4 \times 10^{16}\ cm^{-2}$ in both a:C and a:C–H films. The selected fluence is above the threshold for clustering and nanoparticle formation and below the concentration needed to achieve steady state or significant sputtering loss [4].

The implantation profiles of Co in a:C and a:C–H films were measured with high-resolution Rutherford backscattering spectrometry (HR-RBS) at the National University of Singapore [4,15]. The setup uses a singletron accelerator to focus a 500 keV He^+ beam to a beam spot of 1 mm diameter on the sample target. Particles scattered at an angle of 65° are passed on through an electromagnet to a multichannel plate detector. The electromagnet separates the backscattered particles based on their energy. The energy resolution obtained by this technique is as low as 1 keV [15]. This setup allows accurate measurement of the Co depth profile in the implanted films with 1.1 nm resolution.

The implanted and as-deposited films were further characterised by confocal Raman spectroscopy at Victoria University of Wellington following the data interpretation as developed by Ferrari et al. [14]. The setup uses an Ar ion laser (514.5 nm) as an excitation source. A 100× objective lens was used to focus the laser beam onto the sample. The laser power was limited to 65 μW to prevent heating of the sample. The spectrum was collected for 30 s and each measurement was repeated 5 times to obtain a high signal to noise ratio. The measurements were calibrated with a silicon peak at 521 cm^{-1}. The resolution was found to be less than 1 cm^{-1}.

3. Results and discussion

Raman spectroscopy is a technique widely used to determine the structural properties of carbon films [16]. In the visible wavelength range, DLC has two Raman active modes – both from sp^2 hybridised carbon. The dominant mode originates usually from the stretching of sp^2 bonded carbon atoms. It is denoted as the G peaks (graphite peak) and it is centred around 1500–1600 cm^{-1}. The other mode arises from the breathing mode of 6-folded carbon rings located near dislocations or defects. This peak, referred to as the D peak (disorder peak), is centred around 1300–1400 cm^{-1}.

In this work, Raman spectroscopy was used to identify the nature of implantation induced defects that arise in DLC films during the presence and absence of hydrogen within the films. The Raman spectra were fitted with a double Gaussian peak to extract the details of the D and G peak. The peak position, width and intensity were used to extract structural information of the implanted and as-deposited a:C and a:C–H films [16].

Fig. 1 shows the Raman spectra of the implanted and as-deposited a:C and a:C–H films. Robertson and Ferrari proposed a three stage model correlating the changes observed in the Raman spectra in terms of the G peak position and I(D)/I(G) ratio with a rise in sp^3 content from 0 to 100% [16]. The G peak position and I(D)/I(G) ratio of the implanted and as-deposited a:C and a:C–H films are listed in Table 1.

The three stage model qualitatively attributes the alterations in the Raman spectra to sp^3 character. The first observation is that the as-deposited a:C–H film contains a higher sp^3 content than the as-deposited a:C film due to the higher I(D)/I(G) ratio of the as-deposited a:C film. As per Ferrari and Robertson [16], a change in I(D)/I(G) ratio followed by a corresponding change in the G peak position indicates a change in the sp^3 content of the films. On the other hand, a change in I(D)/I(G) ratio alone indicates a change in just the size and orientation of sp^2 carbon clusters [16]. Upon implantation in both cases we see an increase in the I(D)/I(G) ratio which may denote an increase in sp^2 content and/or cluster size. There is not a significant variation in the G peak position for a:C–H films indicating the variation of the I(D)/I(G) ratio originates predominantly from an increase in cluster sizes of sp^2 carbon [14]. On the other hand, the variation of the I(D)/I(G) ratio of the a:C film upon implantation is accompanied by a shift in the position of the G peak. This suggests that the variation is associated with rehybridisation of sp^3 carbon to sp^2 carbon. This difference in the behaviour of a:C and a:C–H films upon implantation can be attributed to the presence of hydrogen in the a:C–H films which is known to saturate dangling bonds of carbon preventing them from converting to sp^2 hybridisation [11].

Dynamic Transport and Range of Ions in Matter (DTRIM) [17] code was used to simulate the profile of implanted ions in the DLC matrix. The input ions were set to 30 keV Co ions. The profile was computed with an area of 10000 $Å^2$ and 100 layers with an individual layer width of 1 nm. The input fluence was set to $4 \times 10^{16}\ cm^{-2}$. For a:C films, the natural density of carbon, $2.25\ g\ cm^{-3}$ was chosen and for a:C–H films a density of

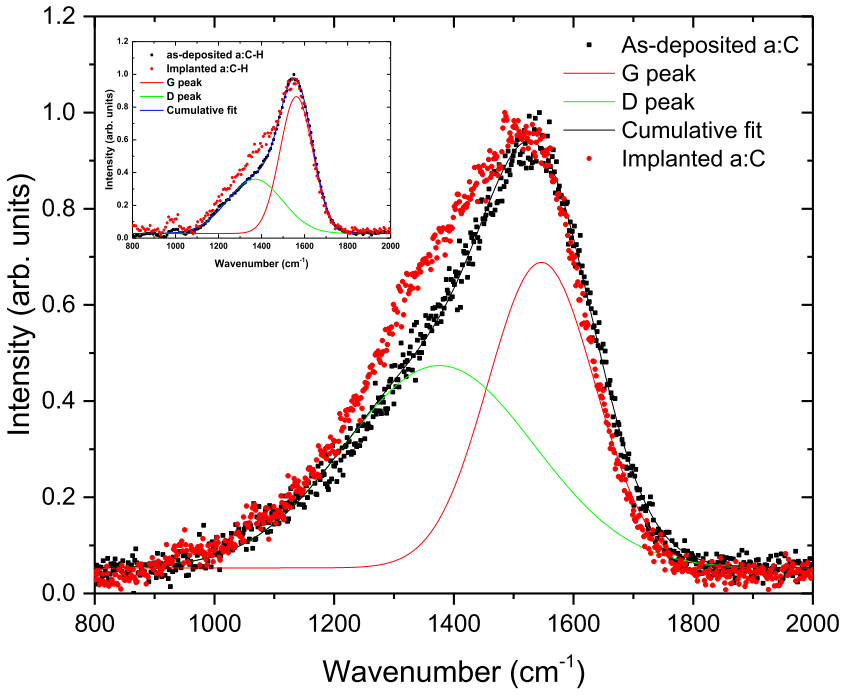

Fig. 1. Raman spectra of as-deposited and Co implanted a:C films. The spectra from a:C–H films are shown in the inset.

Table 1
The parameters obtained by fitting the Raman spectra from as-deposited and implanted a:C and a:C–H films.

Sample number	Film type	G peak position (cm^{-1})	I(D)/I(G) ratio
1	As-dep. a:C–H	1562	0.42
2	Implanted a:C–H	1563	0.76
3	As-dep. a:C	1546	0.67
4	Implanted a:C	1533	0.93

1.51 g cm^{-3} with a C:H stoichiometry of 3:1 was used based on previous data [10].

Fig. 2 shows the implantation profile of Co in a:C and a:C–H films. In both cases, simulations show a unimodal profile with a near Gaussian distribution of Co atoms. The stopping powers from a-C films are expected to be higher than a:C–H films due to a higher density and absence of hydrogen. Consequently, the projected range of Co ions in a:C and a:C–H films are 24 and 37 nm, respectively. While Co in a-C:H films are not expected to reach the surface, in the case of a:C films, a minor fraction of the surface atoms, ~0.5 at.%, is from implanted Co. By fitting the curves to a Gaussian distribution, the full width half maximum of the distribution was calculated to be 21 and 26 nm for a:C and a:C–H films, respectively.

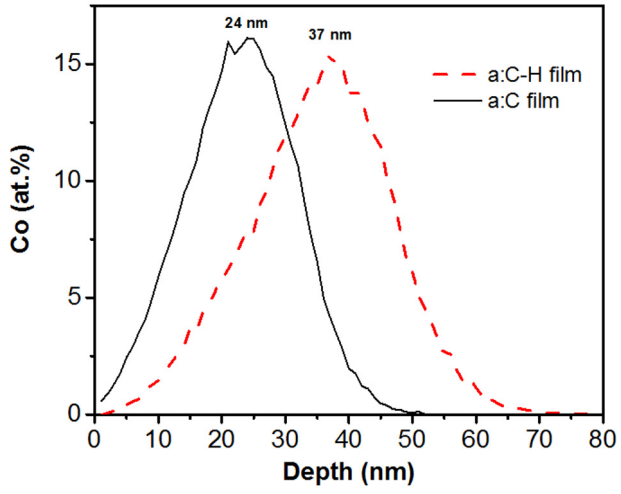

Fig. 2. DTRIM simulation of the Co depth profile in amorphous carbon and hydrogenated amorphous carbon films.

Fig. 3 shows the HR-RBS spectra measured from the Co implanted a:C and a:C–H films. Each spectrum is fit with a SIMNRA simulation to extract the concentration and depth profile [18,19]. The raw data is represented in square symbols and the simulation is represented by a line plot. Fig. 3(a) shows the HR-RBS data and SIMNRA fit for the Co implanted a:C film. The profile while skewed is still Gaussian with a maximum near the projected range predicted by the simulation. The top axis represents the depth scale in nanometres for the Co profile. The depth scale is calculated using stopping power values based on the carbon density of 2.25 g cm^{-3}. A notable feature however is the significant accumulation of Co (2 at.%) at the surface. In the contrast, the representative Co profile measured for the Co implanted a:C–H film shows a bimodal distribution. The depth scale of the Co profile is similarly calculated based on a:C–H density which was determined to be 1.51 g cm^{-3} based on TEM and RBS measurements previously reported [4].

The ion implantation profile of Co in a:C films agree well with simulations. Except for a minor diffusion effect observed at the surface, the profile is unimodal with the average penetration depth matching the projected range calculated by D-TRIM. However, in the case of implanted a:C–H films, the implantation profile does not conform to the D-TRIM simulation. This has been reported earlier in our work, where we explain the observed bimodal distribution as a result of nanoparticle formation, defect generation and diffusion processes enhanced by collision cascades [4].

The results show that Co implantation can lead to bimodal distributions when hydrogen is incorporated in the amorphous car-

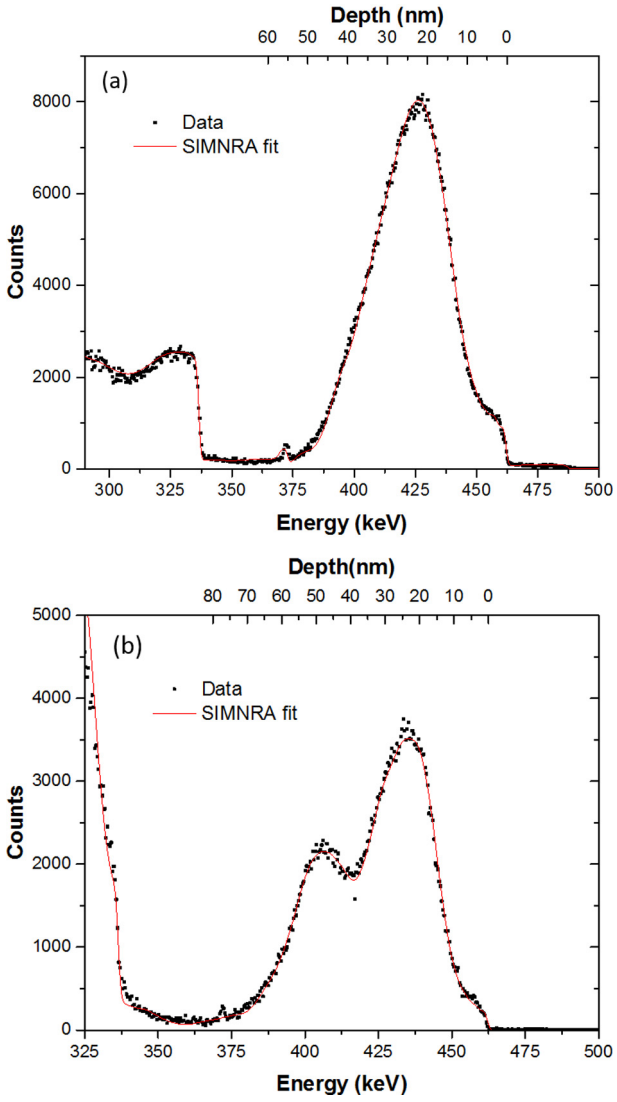

Fig. 3. Comparison of Co depth profiles measured with HR-RBS (symbols, left and bottom axes) of Co implanted amorphous carbon and hydrogenated amorphous carbon (a) Co implanted a:C film and (b) Co implanted a:C–H film. Also shown is a scaled SIMNRA fit to the data (solid curves, top and left axes).

bon matrix. It has been reported by Shamsa et al., that the thermal conductivity of amorphous carbon films reduces significantly, from about 3.5 W $(mK)^{-1}$ to as low as 0.3 W $(mK)^{-1}$, when hydrogen is incorporated into the carbon matrix [7]. This indicates that at the implantation conditions mentioned in this work, i.e., implantation energy and current density, the threshold thermal conductivity value beyond which a bimodal distribution is observed is between 0.3 and 3.5 W $(mK)^{-1}$. This is further evidenced by reports on other thermal insulators [1–3]. At a higher implantation energy, for example 300 keV, and higher current density, for example 60–260 μA cm^{-2}, transition metal implantation into silica and high purity SiO_2 showed a bimodal distribution. These materials have a thermal conductivity in the range of few W $(mK)^{-1}$. However, the reports of ion implantation into SiO_2 for example, at 20 keV do not show a bimodal distribution [6,20].

4. Conclusions

Both, amorphous carbon (a:C) and hydrogenated amorphous carbon (a:C–H) films were prepared by mass selective ion beam deposition. The films were implanted with Co atoms in the near surface region. It has been found that the Co implantation profiles into a:C films agree with the theoretical simulation resulting in near Gaussian shaped profiles. As soon as hydrogen is incorporated in the carbon matrix, in this case to 25 at.%, the implantation profile is measured to be bimodal, which is in disagreement with theoretical simulations. Note, the theoretical model is based on ballistic effects that do not consider thermally enhanced diffusion effects from collision cascades. Incorporating hydrogen in the amorphous carbon matrix decreases the thermal conductivity by a factor of 10 and hence thermal enhanced diffusion effects becomes apparent resulting in a bimodal distribution. Interestingly, even in a:C films the thermal conductivity is still low enough to show minor diffusion of some Co atoms into the surface. This work and previous literature indicate that a threshold value of thermal conductivity exists beyond which transition metal ions can be positioned in a bimodal fashion by making use of diffusion effects from collision cascades. This threshold value however changes with implantation conditions. To the best of our knowledge at implantation conditions as low as 30 keV and 5 μA cm^{-2}, hydrogenated amorphous carbon is the only material that shows a bimodal distribution when implanted at low current and at room temperature without involving any thermal treatments. Additionally, Raman measurements suggest the effects of implantation on diamond-like carbon varies depending on the presence of hydrogen. The data show that Co implantation in a:C films cause significant increase in sp^2 content by rehybridisation of carbon from sp^3 to sp^2 bonding, while in the case of a:C–H films implantation results in a change in the sp^2 cluster size and orientation without major rehybridisation effects.

The results indicate that by tailoring the C:H stoichiometry in the films, it is possible to position Co (magnetic atoms) in the surface of DLC films for applications in magnetic devices.

Acknowledgements

The authors wish to acknowledge the technical assistance of technical staff at GNS Science and at Victoria University of Wellington. This work was supported by the MacDiarmid Institute for Nanotechnology and Advanced Materials, Wellington, New Zealand.

References

[1] T. Höche, T. Angermann, Cross-sectional TEM investigation of tin-implanted SiO_2 glass, J. Non-Cryst. Solids 262 (2000) 114–125.
[2] H. Hosono, H. Fukushima, Y. Abe, R.A. Weeks, R.A. Zuhr, Cross-sectional TEM observation of copper-implanted SiO_2 glass, J. Non-Cryst. Solids 143 (1992) 157–161.
[3] H. Hideo, Simple criterion on colloid formation in SiO_2 glasses by ion implantation, Jpn. J. Appl. Phys. 32 (1993) 3892.
[4] P. Gupta, G.V.M. Williams, R. Hübner, S. Vajandar, T. Osipowicz, K.-H. Heinig, H.-W. Becker, A. Markwitz, Self-assembly of magnetic nanoclusters in diamond-like carbon by diffusion processes enhanced by collision cascades, accepted, Appl. Phys. Lett. (2017), http://dx.doi.org/10.1063/1.4979523.
[5] P. Gupta, H.W. Becker, G.V.M. Williams, R. Hübner, K.H. Heinig, A. Markwitz, Collision cascades enhanced hydrogen redistribution in cobalt implanted hydrogenated diamond-like carbon films, Nucl. Instrum. Methods Phys. Res., Sect. B 394 (2017) 6–11.
[6] J. Leveneur, J. Kennedy, G. Williams, J. Metson, A. Markwitz, Large room temperature magnetoresistance in ion beam synthesized surface Fe nanoclusters on SiO_2, Appl. Phys. Lett. 98 (2011) 053111–053113.
[7] M. Shamsa, W. Liu, A. Balandin, C. Casiraghi, W. Milne, A. Ferrari, Thermal conductivity of diamond-like carbon films, Appl. Phys. Lett. 89 (2006) 161921.
[8] A. Markwitz, B. Mohr, D.F. Carpeno, R. Hubner, Ultra-smooth diamond-like carbon coatings with high elasticity deposited at low temperature by direct ion beam deposition, Surf. Coat. Technol. 258 (2014) 956–962.
[9] A. Markwitz, B. Mohr, J. Leveneur, Room temperature diamond-like carbon coatings produced by low energy ion implantation, Nucl. Instrum. Meth. B 331 (2014) 144–148.
[10] A. Markwitz, P. Gupta, B. Mohr, R. Hubner, J. Leveneur, A. Zondervan, H.W. Becker, Near-surface hydrogen depletion of diamond-like carbon films produced by direct ion deposition, Nucl. Instrum. Meth. B 371 (2016) 230–234.

[11] J. Robertson, Diamond-like amorphous carbon, Mat. Sci. Eng. 37 (2002) 129–281.
[12] P.P. Murmu, A. Markwitz, K. Suschke, J. Futter, A novel radial anode layer ion source for inner wall pipe coating and materials modification-hydrogenated diamond-like carbon coatings from butane gas, Rev. Sci. Instrum. 85 (2014).
[13] K. Suschke, R. Hubner, P.P. Murmu, P. Gupta, J. Futter, A. Markwitz, High energy radial deposition of diamond-like carbon coatings, Coatings 5 (2015) 326–337.
[14] P. Gupta, G. Williams, A. Markwitz, Ferromagnetic order in diamond-like carbon films by Co implantation, J. Phys. D. Appl. Phys. 49 (2016) 055002.
[15] T. Osipowicz, H.L. Seng, T.K. Chan, B. Ho, The CIBA high resolution RBS facility, Nucl. Instrum. Methods Phys. Res., Sect. B 249 (2006) 915–917.
[16] A.C. Ferrari, J. Robertson, Raman spectroscopy of amorphous, nanostructured, diamond–like carbon, and nanodiamond, Philos. Trans. R. Soc. London A: Math., Phys. Eng. Sci. 362 (2004) 2477–2512.
[17] W. Möller, W. Eckstein, Tridyn – A TRIM simulation code including dynamic composition changes, Nucl. Instrum. Methods Phys. Res., Sect. B 2 (1984) 814–818.
[18] M. Mayer, SIMNRA, a simulation program for the analysis of NRA, RBS and ERDA, AIP Conf. Proc. 475 (1999) 541–544.
[19] M. Mayer, Improved physics in SIMNRA 7, Nucl. Instrum. Methods Phys. Res., Sect. B 332 (2014) 176–180.
[20] T. Prakash, G.V.M. Williams, J. Kennedy, S. Rubanov, Formation of magnetic nanoparticles by low energy dual implantation of Ni and Fe into SiO_2, J. Alloy. Compd. 667 (2016) 255–261.